Mater Eng Res, 2022, 4(1): 187-195
DOI: 10.25082/MER.2022.01.001

RESEARCH ARTICLE

# *In-vivo* damage development in Vena Cava Filter: Study of a retrieved device

**Anne Marie Lutz**[1] **Tarun Goswami**[1*]

[1] Department of Biomedical, Industrial and Human Factors Engineering, Wright State University, Dayton, OH 45435, USA



**Correspondence to:** Tarun Goswami, Department of Biomedical, Industrial and Human Factors Engineering, Wright State University, Dayton, OH 45435, USA; Email: tarun.goswami@wright.edu

**Received:** March 22, 2022;
**Accepted:** April 30, 2022;
**Published:** May 6, 2022.

**Citation:** Lutz AM and Goswami T. *In-Vivo* damage development in Vena Cava Filter: Study of a retrieved device. *Mater Eng Ress*, 2022, **4**(1): 187-195. https://doi.org/10.25082/MER.2022.01.001



**Abstract:** This article was prepared from a project assigned in a graduate class, BME 7371, Failure Assessment of Medical Devices, taught at Wright State University by the senior author. The device was donated for the study which was successfully retrieved after 93 days *in-vivo*. Even-though the mechanical integrity of the device held in-tact, the microscopic observations revealed that the damage via corrosion and scratching took place on the surface of the device. The image reconstructed in 3D using image-J software to determine device roughness and depth-of-pits. Results presented in this paper show that damage starts developing in these devices after the implantation that resulted in premature failure in many cases as reported in the media and literature.

**Keywords:** Vana Cava Filter, blood clot and circulation, damage development, pitting

## 1 Introduction

An Inferior Vena Cava (IVC) filter is a device that is placed within the inferior vena cava, which returns blood from the lower half of the body back to the heart. This is a precautionary device which is placed to prevent blood clots from the lung or pelvis from getting into the heart where it could cause a pulmonary embolism or blockage. The device acts as a stopper to catch the blood clots before reaching to the heart. These devices are typically placed when a patient is unable to take blood thinners. Initially IVC filters were permanent implants, however, recently optionally retrievable. Several studies provide the background, yet few studies exist performing the failure analysis with mechanical/material perspective [1–9]. (see Figure 1)

Retrieving the filter requires entry through the Aorta or one of the neck veins pulling the device into a sheath and through the heart. The procedure for retrieval has a much higher risk for complications than the insertion, this is because the filter has sharp legs/tines to keep it in place, so when the filter is sheathed there is a chance the tines can break or may get attached to the IVC. Due to the risk of the procedure, many filters are left behind.

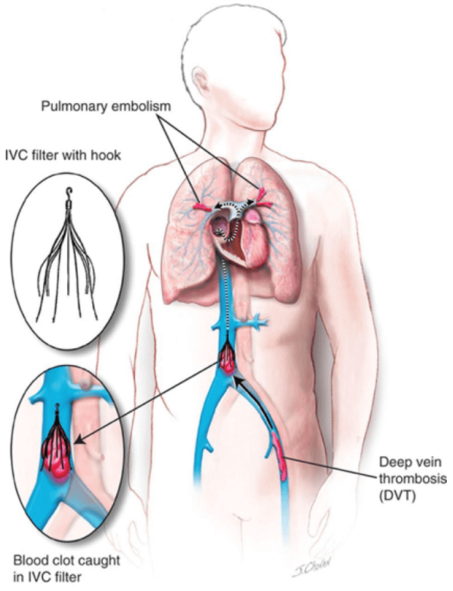


**Figure 1** Schematic of IVC filter placement [1]

A Denali Vena Cava Filter was investigated in this paper. This filter was optionally removable and received FDA clearance in June 2010. It has electropolished cranial and caudal anchors and penetration limiters. It is a conical filter composed of 12 memory struts or tines that are laser cut from a single piece of nitinol (nickel-titanium alloy). The arms were broken into two sections; an upper and lower, which allow for embolic filtration. The two long arms (cranial and caudal) resist inferior and superior migration as well as providing points of incorporation into the wall of the vena cava if the device was left permanently. The device measured 50mm in length, with a maximal diameter of 28mm. The retrieval hook located at the apex was cut from the same piece of nitinol. The filter inserted through the groin or the jugular systems and guided with a 0.035 inch guidewire. Clinical testing was performed through the DENALI trial (ID code NCT01305564, clinicaltrials.gov). There were 21 participating hospitals in the United States [5]. There were 200 patients with 114 screened for filter removal. Three of the patients were denied removal due to presence of thrombosis in the filter. Of the 111 retrieval attempts 108 were successful with a 165 day average of in-vivo duration. In a single center study [9], of 295 filter retrieval attempts in 294 patients 249 were removed successfully that constituted 84.4%. The median in-vivo time was 196 days for successful retrieval compared to 375 days for failed retrieval attempts. 98.6% of the device tines penetrated through the caval wall. Hook and apex, shown in Figure 2 and 3 penetrated to the caval wall for 11.2% of the cases. The segmental failure rates increased the failure rates of overall device 48.4-66.7%, however, without these issues the failure rates lowered 3.9%. Increased failure rates [9] also complicated the procedures. The guideline for the maximum filter tilt was 15%. The long term effects of device implantation remain unknown.

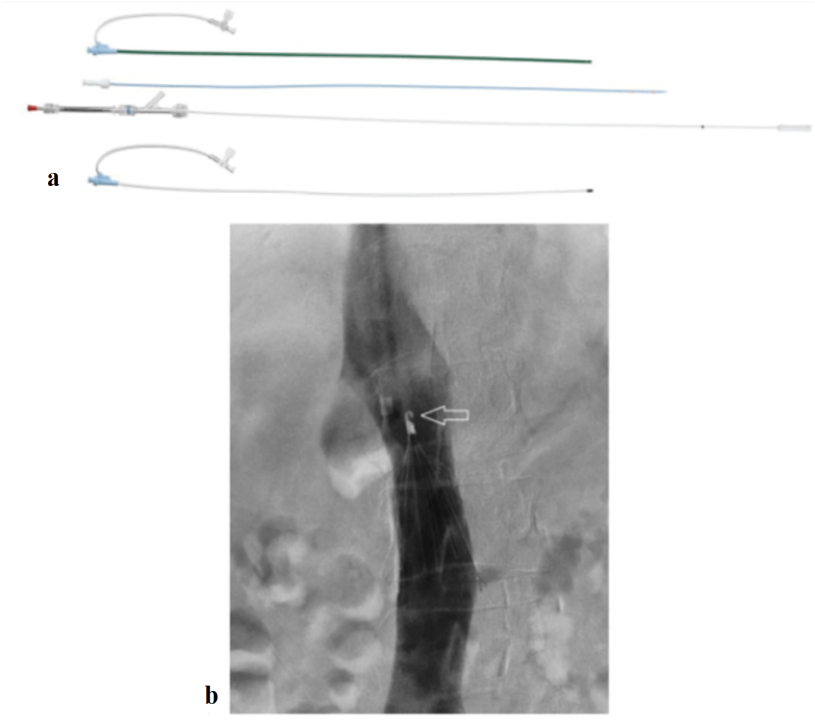


**Figure 2** a) types of guide wires. b) x-ray image of hook location for removal [1]

## 2 Materials and methods

Denali filter is made of nitinol, which is a nickel-titanium alloy. The medical grade nitinol is covered by ASTM F2063 [4]. The device was in-vivo for 93 days. The device was successfully removed without any broken arms or anchors. For this study, damage developed for 93 days of in vivo use were documented. Picture labeling of the device for identification is shown in Figure 1, 2 and 3.

Nitinol contains impurities from carbon and oxygen. This happens during the melting process from the ingots. These impurities are considered inclusions within the metal. These inclusions are an initiation site for fatigue cracks and can promote corrosion of the device. According to ASTM standards, the inclusions must be $<$ 30 micrometers in size and take up $<$2.8% area fractions for alloys with fully annealed Austenite starting temperature of 30 degrees Celsius.

For applications at higher than 30°C, the area fraction negotiated separately. This allows for much more variation because the human body temperature is 37°C. These standards although in place are easier to work around in the medical device field because there is no requirement for multiple melt including vacuum melt and mold steps. Most inclusions for IVC filters are 3 micrometers. Due to this requirement, devices made are for "long term".

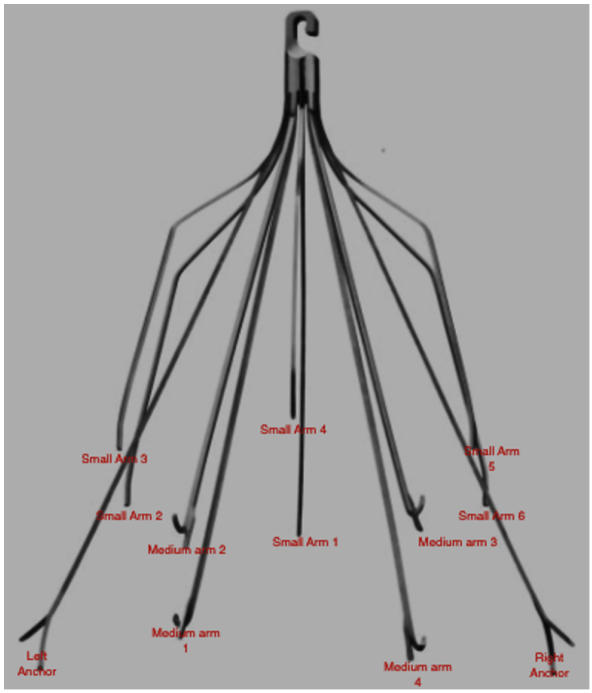


**Figure 3** Device analyzed together with labeling of the hook, tines, and anchor.

**Table 1** ASTM Specification of Nitinol Reference (4)

| Chemical Requirements & Product Analysis Tolerance① | | |
|---|---|---|
| **Element** | **% (mass/mass)** | **Tolerance % (mass/mass)** |
| Nickel | 54.5 to 57.0 | 0.2 under min; 0.2 over max |
| Carbon, maximum | 0.050 | 0.002 |
| Cobalt, maximum | 0.050 | 0.001 |
| Copper, maximum | 0.010 | 0.001 |
| Chromium, maximum | 0.010 | 0.001 |
| Hydrogen, maximum | 0.005 | 0.0005 |
| Iron, maximum | 0.050 | 0.01 |
| Niobium, maximum | 0.025 | 0.004 |
| Nitrogen plus oxygen, maximum | 0.050 | 0.004 for each |
| Titanium② | Balance | n/a |

Notes:
① Product analysis tolerance limits are based on analytical capabilities that have been demonstrated for this composition.
② Approximately equal to the difference between 100% and the sum percentage of the other specified elements. The percentage titanium content by difference is not required to be reported per ASTM F2063.

**Table 2** ASTM standards for element type and tolerance in the nitinol, Source: Reference (4)

| Typical Physical Properties | | | |
|---|---|---|---|
| | Units | Nitinol | Stainless Steel |
| Melting Point | °C<br>*(°F)* | 1310<br>*(2,390)* | 1450<br>*(2,642)* |
| Density | g/cm³<br>*(lb/in³)* | 6.5<br>*(0.235)* | 8<br>*(0.289)* |
| Specific Electrical Resistivity | μΩcm<br>*(μΩin)* | 76 (M) / 82 (A)<br>*(29.9 (M) / 32.3 (A))* | 72<br>*(28.3)* |
| Coefficient of Thermal Expansion | 10⁻⁶/°C<br>*(10⁻⁶/°F)* | 6.6 (M) / 11 (A)<br>*(3.7 (M) / 6.1 (A))* | 17.3<br>*(9.6)* |
| Thermal Conductivity | W/(m °C)<br>*(BTUIT in/sec ft² °F)* | 18<br>*(0.035)* | 16.3<br>*(0.031)* |
| Young's Modulus | GPa<br>*(ksi)* | 40 (M) / 75 (A)<br>*(5,802 (M) / 10,878 (A))* | 193<br>*(27,992)* |
| Ultimate Tensile Strength | MPa<br>*(ksi)* | 1100 - 1500①<br>*(160 - 218)①* | 620 - 2400①<br>*(90 - 348)①* |
| Notes:<br>① UTS can vary greatly depending on heat treatment and alloy.<br>② (M) = Martensite, (A) = Austenite | | | |

# 3 Previous case studies

In a previous study, a 46-year-old woman came in for her 6 month check-up and complained of chest pains. Radiography revealed two fractured components that were identified [7]; one stuck in the pulmonary wall was retrieved successfully and the other in her right ventricle which required an open heart surgery. The failed device showed metal fatigue as the cause of the failure. The patient had morbid obesity (BMI 58.88 kg/m$^2$), had undergone gastric bypass surgery. The filter was implanted before to make sure no thrombosis were present even though the patient had no family history of thrombosis. Below is a picture of the missing arms. (see Figure 4)

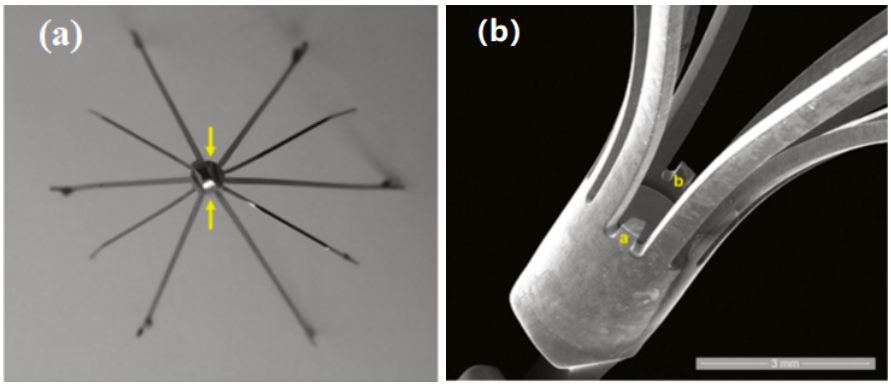


**Figure 4** (a) Missing arms in case study, both medium arms broken at the bottom of hook/apex of device, and (b) scanning electron micrograph showing higher magnification [7].

When compared to other filters the Denali retrieval has the best retrieval rate ratio without complications. The FDA states that if there is no longer a need for the IVC filter to be implanted, then the device should be removed. This prevents any material failure from happening over time while the device is implanted.

# 4 Results and discussion

Denali case studies in the literature show metal fatigue, where fracture occurred from one or more of the small and medium arms failing near the apex. Since the device under investigation was mechanically in-tact and we were limited to surface topological investigation only from the donor, we could not perform cut-up evaluation showing microstructure and damage development via dislocation structures. Since similar devices failed from the regions of hook/apex, we chose

to study that area for each tine. Below are images that were taken using the optical microscope. Even though it was very difficult to position the device in the microscope to document damage development, we observed that each tine was damaged, where pitting and scratching observed. We chose to present select few tines showing these damages in Figure 5 and 6, respectively. Device was *in vivo* for 93 days and each tine exposed to uniform conditions. Since we do not know of the pitting kinetics and other conditions, we will not discuss the growth rates therefore, the features identified are presented. All the regions in the filter, immediately below the hook showed pitting and scratching taking place. It is likely that machining those edges may have left residual stresses and may be speculated to have thermal distortion, together with inclusions resulted in pitting corrosion. Since the device is positioned in the blood flow direction and those contacts are showing to be eroding the filter tine surfaces. As a result the scratches generate. Since the depth of the pitting is higher than those of scratches, it is likely that pit, upon reaching a critical size, may transition to fatigue. An aspect ratio of 1 was connected to be a transition criterion [10], thus corrosion fatigue may be concluded for the failed tines.

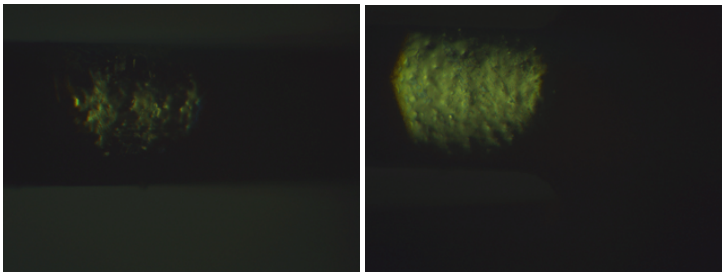

(a) Left Anchor Pitting (b) Medium arm discoloration and pitting

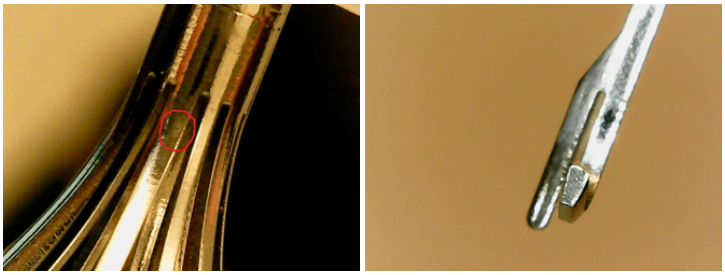

(c) Circled is a large pit and other corrosion damage through the length (d) Medium arm 1 hook

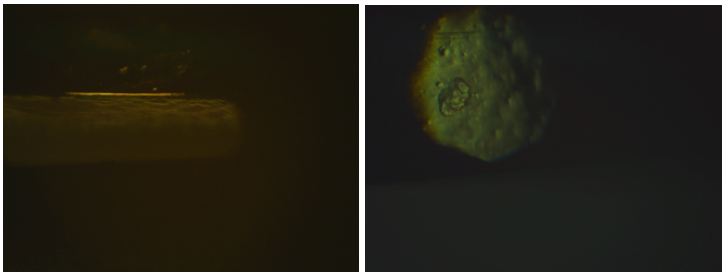

(e) Medium arm 4, pitting and scratches near the apex (f) Right anchor, appears to be an inclusion along with pitting

**Figure 5** Microstructural details of the damage in various locations of the filter

(a) Small arm 6 near apex larger pits (b) Same area as (a) showing pitting

**Figure 6** Identifying area for further analysis and method development

We developed a method to further process the images presented above in Figure 6. Image was analyzed using Image-J, the area of the lighted portion, in terms of the mean, min, and max. It is possible to determine how many pits are in the material, and how deep the pits are. This analysis is at one spot at the small arm 6 near the apex.

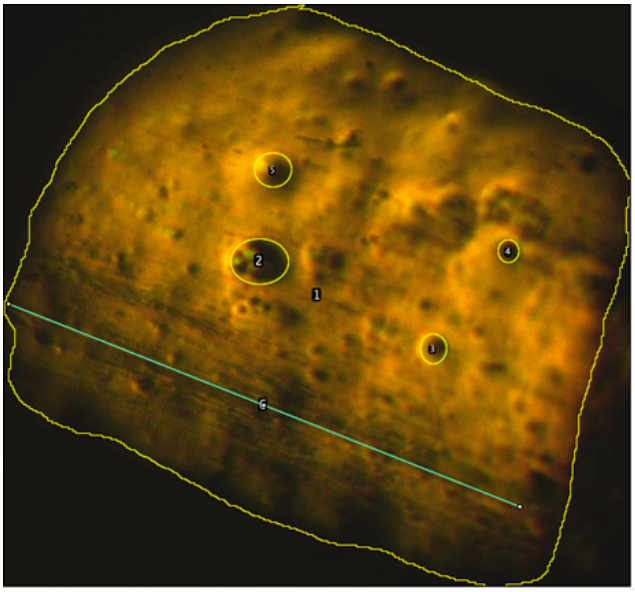


**Figure 7** Image of small arm 6, with labeling of scratches and pits

**Table 3** Summary of analysis at Small arm 6 of the pitting and scratches

| No. | Label | Area | Mean | Min | Max | Angle | % Area | Length |
|---|---|---|---|---|---|---|---|---|
| 1 | SA6 Large pit.jpg | 241293 | 67.88 | 21 | 163 | 0 | 0 | 0 |
| 2 | SA6 Large pit.jpg | 1940 | 55.96 | 24 | 155 | 0 | 0 | 0 |
| 3 | SA6 Large pit.jpg | 577 | 83.99 | 31 | 142 | 0 | 0 | 0 |
| 4 | SA6 Large pit.jpg | 344 | 52.8 | 28 | 96 | 0 | 0 | 0 |
| 5 | SA6 Large pit.jpg | 928 | 80.96 | 30 | 163 | 0 | 0 | 0 |
| 6 | SA6 Large pit.jpg | 533 | 47.82 | 27.33 | 78.3 | -21.6 | 0 | 532.4 |

The area and length of the scratches and pits listed above while the roughness with statistical analysis is listed below.

**Table 4** Calculated roughness of the surface

| Slice | Rq | Ra | Rsk | Rku | Rv | Rp | Rt | Rc | FPO | MFOV | FAD | MRV | SA |
|---|---|---|---|---|---|---|---|---|---|---|---|---|---|
| 1 | 30.63 | 26.28 | 0.85 | -0.41 | 19.67 | 163.33 | 143.67 | 50.42 | 40.32 | 31.96 | 57.23 | 0.02 | 2.21 |

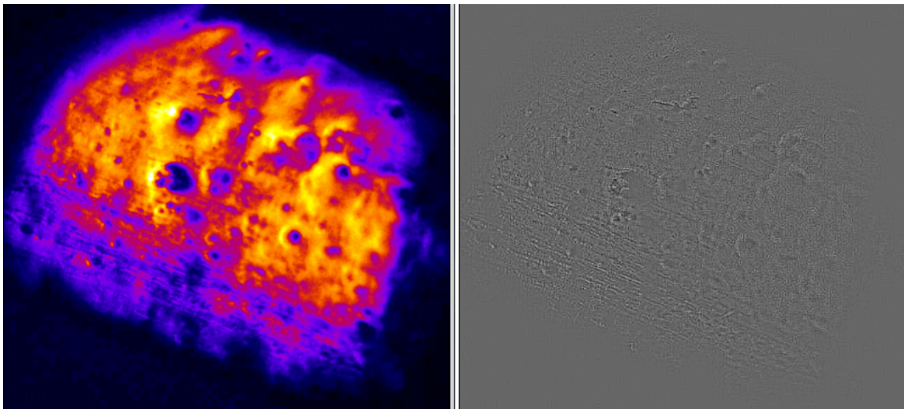

**Figure 8** Waviness and Surface Roughness at the same location, small arm 6.

Above are the waviness and roughness isolated from the rest of the image. Adjacent is the Surface area plot in which we can see the depth of the pits and scratches in Figure 9.

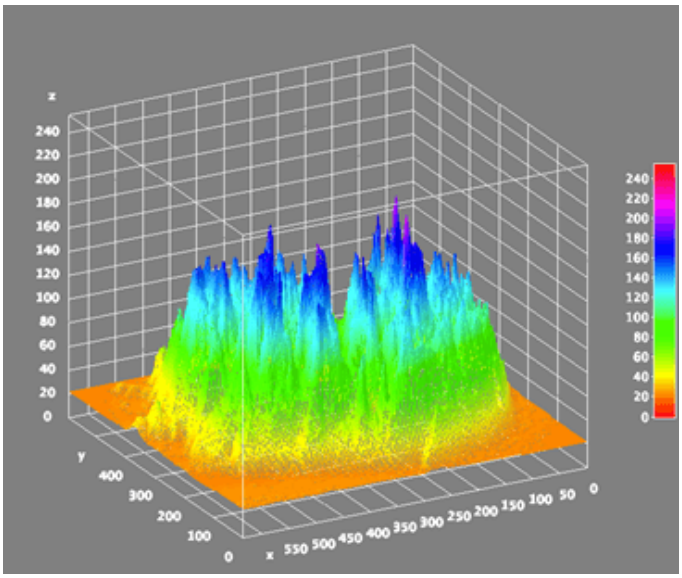


**Figure 9** Surface plot of the Images above, the pitting is shown through the depth

The same method was applied to another location and image showing damage development analyzed below.

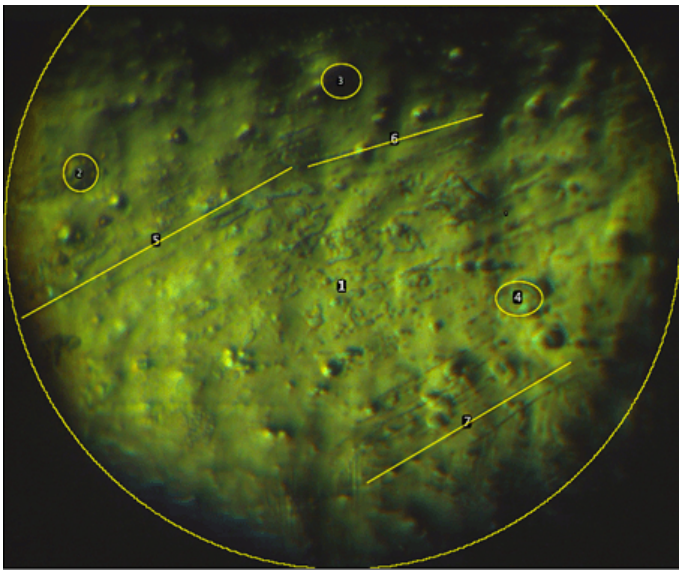


**Figure 10** Image of Analysis of Medium Arm 4

**Table 5** Summary of analysis at Medium Arm 4 of the pitting and scratches

| No. | Label | Area | Mean | Min | Max | Angle | % Area | Length |
|---|---|---|---|---|---|---|---|---|
| 1 | Medium arm 4 Scratch/pit | 530202 | 64.7 | 24 | 188 | 0 | 0 | 0 |
| 2 | Medium arm 4 Scratch/pit | 1700 | 53.2 | 37 | 86 | 0 | 0 | 0 |
| 3 | Medium arm 4 Scratch/pit | 1803 | 34.9 | 28 | 76 | 0 | 0 | 0 |
| 4 | Medium arm 4 Scratch/pit | 2120 | 86.76 | 48 | 140 | 0 | 0 | 0 |
| 5 | Medium arm 4 Scratch/pit | 398 | 73.83 | 29.26 | 109 | 29 | 0 | 396.9 |
| 6 | Medium arm 4 Scratch/pit | 235 | 63.38 | 35.37 | 138.24 | 16.65 | 0 | 233.71 |
| 7 | Medium arm 4 Scratch/pit | 305 | 67.21 | 39.89 | 102.18 | 30.44 | 0 | 303.67 |

Table 5 shows the length and area of major pits and scratches.

**Table 6** Surface roughness for, Medium Arm 4, Figure 10

| Slice | Rq | Ra | Rsk | Rku | Rv | Rp | Rt | Rc | FPO | MFOV | FAD | MRV | SA |
|---|---|---|---|---|---|---|---|---|---|---|---|---|---|
| 1 | 28.36 | 24.52 | 0.56 | -0.77 | 23 | 187.67 | 164.67 | 58.85 | 47.49 | 25.56 | 152.49 | 0.048 | 2.17 |

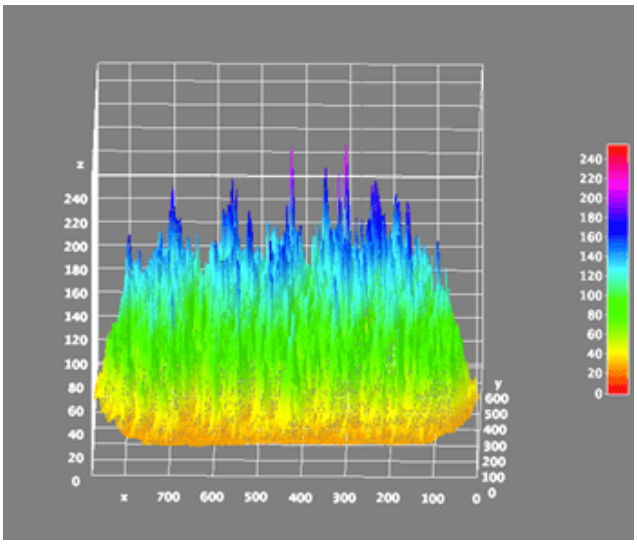


**Figure 11** Surface plot of the image in Figure 10

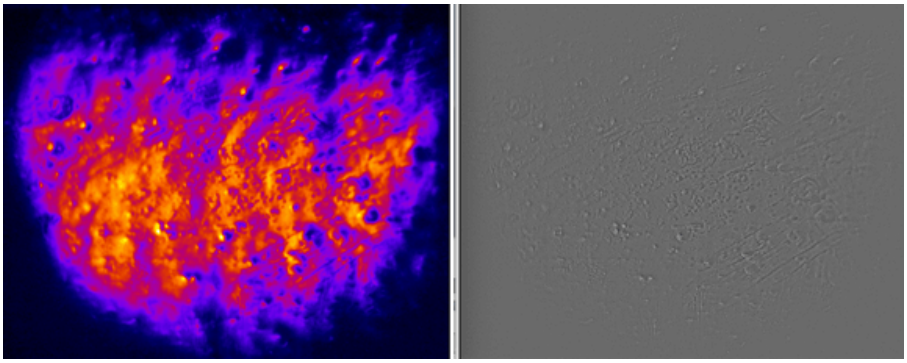

**Figure 12** Waviness and Roughness using Image-J plug-in

Since the Ra is the measure of surface peaks and valleys, it is the arithmetic average of the height deviation in the profile shown in Table 4 and 6 is 26. Even though the bacterial infection on these devices found to be rare in literature, if the roughness increases a certain value, those bacterial sites can find a foothold in those locations. Figure 9 and 11 show the 3D plot of the pits, it is apparent the depth of the pits exceeded 150-240 $\mu$m. From the limited information that we have on the device, we cannot isolate if an increase in application temperature, from 30 to 37°C caused the material to creep. Cavitation is one of the ways the damage develops under creep conditions and may be manifested in terms of the pits. Both pitting corrosion and creep cavitation are uniformly distributed damage, it is likely that their interactions produced more damage as documented in Figure 9 and 11.

From this analysis, we are able to postulate that the metal tines on the Denali filter are deteriorating from the *in vivo* exposure where damage development is in terms of pitting, scratching and discoloration. Pitting taking up much more area, assuming them occurring from the sites of inclusions, than is recommended by the standards given by the FDA. Even though the devices were retrieved at several sites due to clinical relevance, there is a need for in-depth study using these frameworks as well as dislocation evolution and fatigue cracking from the sites of the pit(s). Further analysis should be done in order to look into the total surface area of each metal arm to find out the exact area which is affected by the pitting. It may be possible to conclude that the pitting corrosion together with possible cavitation may have caused device failure if the device had been left *in vivo*. The image processing proves that the failure would have occurred near the hook of the device which is where failure occurs in other case studies specifically with this device.

# 5 Conclusion

The analysis of this device shows that although the device did not break, the damage developed at the base of each tine under the hook from pitting corrosion, scratching by erosion

and possible creep cavitation. Scratches and discoloration occurred from the exposure to blood flow. The prevalence of pitting, scratches and discoloration from each of the tines may indicate other dominating factors such as creep, manufacturing and materials issues in the construction of the device. Nitinol is not supposed to be textured and in the process of making the filters it is highly unregulated. A continuation of this investigation would be recommended to look into inclusion characterization and dislocation structure so that creep/fatigue initiation issues understood more accurately resulting in corrosion fatigue failure of the tines.

# References


[1] Carroll S and Moll S. Inferior Vena Cava Filters, May-Thurner Syndrome, and Vein Stents. Circulation, 2016, **133**: e383-e387.
https://doi.org/10.1161/CIRCULATIONAHA.115.019944

[2] Caplin DM, Nikolic B, Kalva SP, *et al*. Society of Interventional Radiology Standards of Practice Committee, Quality improvement guidelines for the performance of inferior vena cava filter placement for the prevention of pulmonary embolism. Journal of Vascular and Interventional Radiology, 2011, **22**: 1499-1506.
https://doi.org/10.1016/j.jvir.2011.07.012

[3] US Food and Drug Administration. Removing Retrievable Inferior Vena Cava Filters: FDA Safety Communication, May 6, 2014.
https://www.fda.gov/medical-devices/medical-device-safety/safety-communications

[4] Alloys C, Technique F, Inductively S, *et al*. Standard Specification for Wrought Nickel-Titanium Shape Memory Alloys for Medical Devices and Surgical Implants 1, 2005.

[5] William TK and Scott W. Robertson. Bard Denali Inferior Vena Cava Filter Fracture and Embolization Resulting in Cardiac Tamponade: A Device Failure Analysis. Journal of Vascular and Interventional Radiology, 2015, **26**(1): 111-115.
https://doi.org/10.1016/j.jvir.2014.08.001

[6] Majdalany BS, Khaja MS and WilliamS DM. Bard Denali Filter Fractures. Journal of Vascular and Interventional Radiology, 2016, **27**(7): 1099-1101.
https://doi.org/10.1016/j.jvir.2016.04.008

[7] Sathyanarayana R, Tan G, Tonder FV, *et al*. Bard DENALI Inferior Vena Cava Filter: Another "Arm" Fracture. Journal of Vascular and Interventional Radiology, 2016, **27**(11): 1722-1724.
https://doi.org/10.1016/j.jvir.2016.05.025

[8] Veverkova J, Bartkova D, Weiser A, *et al*. Effect of Ni ion release on the cells in contact with NiTi alloys. Environmental Science and Pollution Research, 2020, **27**(8): 7934-7942.
https://doi.org/10.1016/10.1007/s11356-019-07506-8

[9] Morrow KL, Bena J, Lyden SP, *et al*. Factors predicting failure of retrieval of inferior vena cava filters. 2019. Journal of Vascular Surgery: Venous and Lymphatic Disorders, 2020, **8**(1): 44-52.
https://doi.org/10.1016/j.jvsv.2019.07.010

[10] Goswami T and Hoeppner DW. Transition Criteria - From a Pit to a Crack. Journal of the Mechanical Behavior of Materials, 1999, **10**(5-6): 261-278.
https://doi.org/10.1515/JMBM.1999.10.5-6.261